JOURNAL OF THERMOPHYSICS AND HEAT TRANSFER
Vol. 21, No. 1, January–March 2007

Analysis of Chemical Nonequilibrium and Elemental Demixing in Plasmatron Facility

M. Panesi* and P. Rini†
Von Kármán Institute for Fluid Dynamics, 1640 Rhode-St.-Genèse, Belgium
G. Degrez‡
Université Libre de Bruxelles, 1050 Bruxelles, Belgium
and
O. Chazot§
Von Kármán Institute for Fluid Dynamics, 1640 Rhode-St.-Genèse, Belgium

DOI: 10.2514/1.25378

A detailed numerical analysis is performed in the torch and in the test chamber of an inductively coupled plasma facility. The main purpose is the analysis of the plasma jet in the test chamber and the assessment of its degree of nonequilibrium together with the level of elemental demixing. To this end three different mathematical formulations have been used: an extended chemical nonequilibrium formalism including finite-rate chemistry and two forms of equation valid in the limit of local thermochemical equilibrium, i.e. the equilibrium formulation with variable elemental fractions, which takes into account the demixing of chemical elements and the classical formulation, where the molar fraction of elements is supposed to be constant. To assess the influence of the finite-rate chemistry model on the results, two models have been used. Simulations at various operating pressures indicate that the model dependency is strongly reduced at sufficiently high pressures (above 10 kPa) while relevant at lower pressure. As the operating pressure is increased, chemistry becomes increasingly fast and the nonequilibrium results correctly approach those obtained assuming local thermochemical equilibrium, provided that elemental fraction variations are correctly taken into account.

Nomenclature

k_f	=	forward reaction rate
M_i	=	molar mass of species i
N_{el}	=	number of elements
N_{sp}	=	number of species
p	=	mixture pressure
T	=	mixture temperature
$\boldsymbol{u}$	=	mixture velocity
X_c	=	volumetric fraction of element c
x_s	=	mole fraction of species s
ρ	=	mixture density

I. Introduction

THE numerical modeling of chemical reacting plasma flows, requires the solution of the well-known Navier–Stokes equations complemented by additional conservation equations. The number of equations needed, in general, depends on the assumptions made and on the degree of approximation used in the modeling of the physical phenomena, and can be large in sophisticated approaches such as state to state [1] or collisional radiative [2,3] models. An approximation of the chemico-physical processes is constituted by the chemical nonequilibrium approach that requires the solution of a conservation equation for each species of the mixture. This system of equations is often hard to implement and solve numerically. In addition, many physical parameters essential for the modeling of kinetic and chemical processes in the gas mixture are usually not available. For these reasons, when chemistry and energy exchanges are fast, it is usually preferable to solve the more elegant and unambiguous local thermochemical equilibrium (LTCE). It is common practice in aerospace sciences to compute LTCE flows, assuming a fixed elemental composition [4]. Care should be taken when comparing these results with nonequilibrium calculations, for which demixing [4–6] of elements does occur. The results to be presented clearly show that as pressure is increased and equilibrium conditions are approached, differences between the fixed elemental fraction LTCE model and nonequilibrium model [7] persist; however, when variations of elemental composition are correctly allowed for in the LTCE model, a better agreement is found.

This paper is inspired to the analysis performed by Rini et al. [8]. There the authors present an accurate analysis of the demixing phenomena in the von Kármán Institute for Fluid Dynamics (VKI) Plasmatron torch [9], whereas here the core of the analysis is moved to the physico-chemical characterization of the jet flowing the test chamber for air plasmas. This will allow us to draw some conclusions concerning the degree of demixing in the area of the chamber where experiments to determine catalytic properties are carried out.

Moreover, beside the elemental diffusion, the new numerical analysis performed allows the assessment of one of the basic assumption in the Institute for Problems in Mechanics (IPM) methodology [10]. This approach (used to estimate the catalytic properties of thermal protection system materials) supposes in fact thermochemical equilibrium conditions to be established in the torch and in the test chamber. However, there is no proof in the literature that equilibrium [11] conditions exist and a detailed analysis assessing the quality of this assumption is not available. To address this need we present both chemical nonequilibrium and chemical equilibrium computations to determine a range of pressure in which

Presented as Paper 2896 at the 37th AIAA Plasmadynamics and Lasers Conference, San Francisco, 5–8 June 2006; received 23 May 2006; revision received 23 July 2006; accepted for publication 23 July 2006.

*Ph.D. Candidate, Department of Aeronautics and Aerospace, 72, Chaussée de Waterloo; also assistant at Service de Mécanique des Fluides, Université Libre de Bruxelles; panesi@vki.ac.be. Member AIAA.

†Ph.D. Candidate, Department of Aeronautics and Aerospace, 72, Chaussée de Waterloo; also assistant at Service de Mécanique des Fluides, Université Libre de Bruxelles; pietro.rini@gmail.com. Member AIAA.

‡Professor, Service de Mécanique des Fluides, Université Libre de Bruxelles; also adjunct Professor, von Kármán Institute, Department of Aeronautics and Aerospace, 72, Chaussée de Waterloo; gdegrez@ulb.ac.be.

§Professor, Department of Aeronautics and Aerospace, 72, Chaussée de Waterloo; chazot@vki.ac.be.

equilibrium computations are as accurate as those obtained under chemical nonequilibrium, using two finite-rate chemistry models. The investigation of the validity of the equilibrium assumptions previously mentioned represented the main motivation and objective of the present research activity.

The manuscript is organized as follows. Before presenting the results of our study we recall the main aspects of the physico-chemical models used in the simulation. Then we define the geometrical configuration considered, highlighting the need for additional boundary conditions with respect to previous investigations [8] to be used in the test chamber. Finally, the result section is divided in two parts: 1) a qualitative analysis of the finite-rate chemistry model, and 2) a qualitative and detailed investigation of the flow behavior for all the operating pressures.

The first part is focused on the influence of the kinetic model carried out comparing temperature and oxygen elemental fraction contours.

The second part is devoted to a more accurate analysis, in which the main physico-chemical properties of the flow are identified extracting temperature and elemental molar fraction profiles in several crucial parts of the computational domain.

II. Physico-Chemical Modeling

When performing calculations with chemically reacting flows, in addition to the equations expressing the conservation of mass, momentum, and energy [12], the knowledge of the composition is needed to retrieve the transport and thermodynamic properties of the mixture to close the system of equations. For this purpose, in this section, different physico-chemical models are briefly recalled. The interested reader can find a more extensive description in [8] where the authors describe in detail the models used for the treatment of electromagnetic field and for the flowfield.

A. Chemical Composition

It is well known how chemical processes take place by molecular collision or radiative interactions. Hereafter we just focus on the molecular interaction due to collisions. In this case the determination of the composition is, in general, done by writing conservation equations for each species present in the mixture. From a careful analysis of these equations, we can identify at least two chemical regimes depending on the relative magnitude of the convective (diffusive and chemical) source terms: 1) chemical nonequilibrium and 2) chemical equilibrium conditions.

1. *Chemical Nonequilibrium (CNEQ)*

Under chemical nonequilibrium conditions, differential equations describe the advection, diffusion, and chemical processes make the species concentrations vary within the flowfield. Note that these equations are written for heavy particles only. Indeed, when charged species are to be considered, we obtain the electron mole fraction by explicitly imposing quasi-neutrality $x_e - \sum_{\text{ions}} x_s = 0$. The mass production terms, present in the species continuity equations, are computed using the law of mass-action [13] and require the knowledge of the rates for all the reactions needed to describe the flow behavior. Values of these rates for high-temperature air are available in literature, but they have a relatively large uncertainty. Hence any nonequilibrium analysis is strongly affected by the trustworthiness of the existing rate data. In the present work two different models for the forward reaction rates coefficient have been analyzed, i.e., the Park [14] and Dunn–Kang [15] models. These models give rates values for the forward reaction rates, and in the present study the backward reaction rates have been retrieved making use of the equilibrium constant, according to the principle of detailed balance [13].

2. *Differences Between the Two Finite-Rate Chemistry Models*

The two kinetic models differ significantly in terms of number of elementary reactions considered and in terms of rate constants. A direct analysis of the concentration profiles, proposed in [16], shows that the main differences between the two models concern the deionization reactions of N^+ and O^+ in the jet area. This is due to the fact that both reaction sets describing charge exchange and ionization and the reaction rates coefficients in these sets are very different [15].

3. *Chemical Equilibrium*

When chemistry is sufficiently fast, equilibrium conditions are achieved and this simplifies considerably the complexity of the flow description. The composition satisfying the species equations in the limit of local equilibrium conditions is coincident with the solution of the nonlinear system under these conditions. In this framework, in [8] the authors introduce two regimes used to describe the equilibrium conditions, recalled hereafter.

1) LTCE, constant elemental fraction (LTCE-CEF): The mixture composition is computed in all the domain discretization as a function of pressure and temperature assuming constant elemental fraction equal to the inlet ones.

2) LTCE, variable elemental fraction (LTCE-VEF): The composition is obtained as a function of the local pressure, temperature and elemental fractions, the latter being obtained by solving a set of chemical element continuity equations.

B. Governing Equations and Boundary Conditions

The governing equations and the numerical techniques used in this manuscript to describe the dynamic of plasma flowing in an inductively coupled plasma (ICP) facility is the same as the one presented in [8–17]. However, a different configuration is considered in the following, including both the torch and the test chamber of the VKI Plasmatron. As a consequence, additional boundary conditions have been introduced, a description of which is to be presented shortly. To simulate tests of thermal protection material (TPM) samples held in the test chamber, we should ideally consider the plasma flow behavior in the torch and in the whole chamber simultaneously. To reduce the computational time, Magin [18] suggested to consider only a subdomain of the chamber containing the hot-jet impinging on a probe, instead of extending the computational domain until the chamber outer walls and exit. This simplifies considerably the solution of the problem still conserving the importance of the obtained results, because the region richest in physics corresponds to the hot-jet and certainly not to the cold recirculation zone present at higher radius [19]. A validation of this boundary condition can be found in [20], where the numerical solution of the whole chamber is compared with the one on a reduced domain, confirming the validity of the approach at least for these operative conditions.

In the framework of the research presented in this paper we just performed the analysis of the hot-jet, without the presence of a probe, as shown in Fig. 1a. By analyzing Fig. 1a, we notice the need to define a boundary condition for the axis of symmetry (c), the eastern boundary (b) in the chamber, the quartz tube wall (f) and a part of the chamber wall (f), the torch inlet (d), and the northern boundary in the chamber (a).

1. *Northern Boundary in the Chamber*

It is well known that for subsonic flow conditions, the pressure in the test chamber of ICP facilities is almost constant, especially when no probe is placed in it. For this reason we built the mesh cutting in the chamber at a certain radius (14 cm) without including the outer wall in the domain discretization. This introduces an additional boundary (a) on which we impose the following conditions. The value of the state variables, except pressure and species concentrations in case of CNEQ (or elemental fraction in case of LTCE-VEF), is extrapolated from the inner field. The pressure on the other hand is imposed and it is supposed to be constant along the whole boundary. The species concentration (in case of CNEQ or the elemental composition in case of LTCE-VEF) is fixed and it is equivalent to the LTCE-CEF molar composition 79%N_2 and 21%O_2 (or 79%N and 21%O for LTCE-VEF). In the three formulations we have that

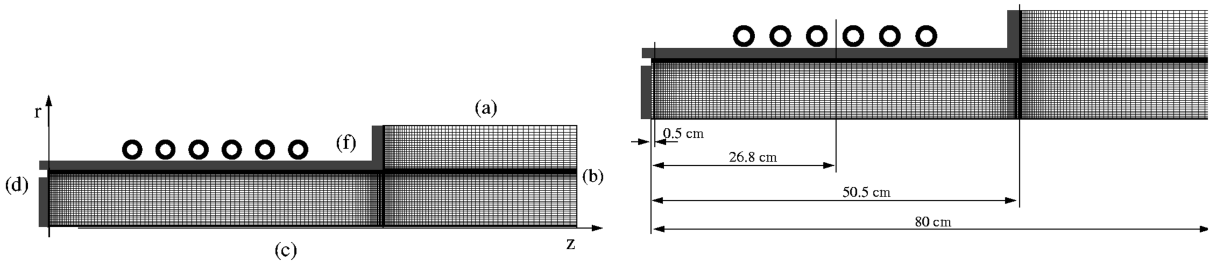

a) Computational domain with its boundaries

b) Location of the sections investigated in the computational domain

Fig. 1 Boundary conditions and sections in the computational domain.

In case of CNEQ:

$$x_{N_2} = 0.79; \qquad x_{O_2} = 0.21$$

In case of LTCE-VEF:

$$Y_{N_2} = 0.76; \qquad Y_{O_2} = 0.24$$

Moreover

$$\frac{\partial \rho \boldsymbol{u}}{\partial n} = 0; \qquad \frac{\partial T}{\partial n} = 0; \qquad p = p_A$$

where p_A stands for the ambient pressure in the chamber.

2. Torch Inlet

The flow is injected through a thin ring near the torch wall. The axial inlet momentum Q is to be calculated from a given total mass injection rate. This translates into the following inlet boundary condition:

$$\frac{\partial p}{\partial z} = 0; \qquad \rho u = Q; \qquad \rho v = 0; \qquad \rho w = 0; \qquad T = T_A$$

$$\text{CNEQ: } x_s = x_{A,s}; \qquad \text{LTCE-VEF: } Y_c = Y_{A,c}$$

where the temperature, the composition, and the elemental mass fractions of the (cold) ambient gas fed to the torch are indicated as T_A, $x_{A,s}$, and $Y_{A,c}$ respectively. In the ICP torches for TPM testing simulated here, the central inlet is generally removed and replaced by a solid wall (Fig. 1a); there, we impose an adiabatic no-slip condition:

$$\frac{\partial p}{\partial z} = 0; \qquad \rho \boldsymbol{u} = 0; \qquad \frac{\partial T}{\partial z} = 0; \qquad \text{CNEQ: } \frac{\partial x_s}{\partial z} = 0$$

$$\text{LTCE-VEF: } \frac{\partial Y_c}{\partial z} = 0$$

3. Eastern Boundary in the Chamber

This boundary condition is a consequence of the implicit assumption that the area of the chamber behind the sample has a negligible influence on the test area and can therefore be excluded from the numerical simulation.

This is done imposing

$$\frac{\partial p}{\partial n} = 0; \qquad \frac{\partial \rho \boldsymbol{u}}{\partial n} = 0; \qquad \frac{\partial T}{\partial n} = 0; \qquad \text{CNEQ: } \frac{\partial x_s}{\partial z} = 0$$

$$\text{LTCE-VEF: } \frac{\partial Y_c}{\partial z} = 0$$

C. Thermodynamic and Transport Properties

A detailed overview of the thermodynamic and transport property models used has been given in previous works on LTCE air plasmas [17,21,22].

Quantum physics describes how molecules and atoms store the energy in different modes, each of which is quantized. In the present work the thermodynamic properties have been computed considering the internal modes of the different species and making the assumption of rigid harmonic oscillator for the diatomic molecules. In such case the rotational, vibrational, and electronic energy modes are considered independent from each other and thermodynamic properties of individual species (and of the mixture) follow from straightforward statistical mechanics considerations [13]. Moreover, only a finite number of electronic levels need to be taken into account [21] and here we consider the strictly minimum number of electronic levels that produces a non-negligible change of energy in the temperature range of interest in this research ($T < 20,000$ K).

Transport properties are computed following the Chapman–Enskog method [21]. The viscosity and heavy particle thermal conductivity are computed with the mixture rules of Yos as listed by Gupta et al. [23]. The rotational, vibrational, and electronic thermal conductivities are modeled by means of the Eucken approximation [23]. The electron thermal conductivity and electrical conductivity are computed with the formulas due to Devoto [24], where two nonvanishing Sonine polynomial contributions were found to yield accurate results [21].

The diffusion fluxes have been computed solving the well-known Stefan–Maxwell system [25,26] of equations which consists of a linear system (in the diffusion fluxes) of as many equations as the chemical species in the mixture, supplemented by the auxiliary condition that the sum of the diffusion fluxes is zero plus the ambipolar constraint [27,28]. They are perfectly equivalent, by derivation, to the complete diffusion equations, but remarkably less computationally expensive than the latter.

D. Mixture Definition

As mentioned and justified in [28] we represent the air plasma by a mixture of 11 chemical components, suited for Earth entry applications [23,29]. Neutral species are O_2, N_2, O, N, and NO. Charged species are NO^+, O^+, N^+, O_2^+, N_2^+, and e^-.

The composition of this mixture is obtained as discussed previously depending on the chemical regime considered.

III. Characterization of the Flow in the Jet

The results to be presented shortly concern both the investigation of the torch and the hot exhaust jet in the chamber. As briefly discussed in the introduction, the forthcoming results will allow to verify for which operating conditions of the VKI Plasmatron, the numerical simulation of LTCE plasma flows is as accurate as the chemical nonequilibrium one, both in the torch and especially in the test chamber. The consequences of this finding will have a direct impact on the range of applicability of the methodology used for the estimation of catalytic properties of thermal protection system materials [10].

The mesh used for the solution of the flowfield equations is divided into two blocks: the first one (112 by 44 cells) is used to discretize the domain within the torch, whereas the second block (60 by 67 cells) reproduces a part of the test chamber. Grid resolution studies have moreover confirmed that the grid is sufficiently fine and the solution is not therefore mesh dependent. In particular, the grid accuracy for

the first block have been already analyzed in [8] and therefore it has not been object of analysis in this research project. For the second block different grid densities have been tested, leading to the conclusion that the dependency of the results on the grid refinement disappears already for a coarser mesh (30 by 34). As an example, and only for illustrative purposes we present in Fig. 5d a comparison between the results obtained with the two grids (30 by 34) and (60 by 67) in terms of temperature profiles.

The operating conditions, selected as representative of Earth entry, are recalled as follows: ambient and wall temperature, 350 K; power injected into the plasma, 80 kw; frequency, 0.37 MHz; inlet swirl, 0 deg; mass flow, 8 g/s; and operating pressures, 5, 10, 20, and 30 kPa.

For each simulation, the three chemical regimes, CNEQ, LTCE-CEF, and LTCE-VEF, have been considered. The presentation of the results is organized in two parts. Firstly, we present a qualitative analysis based on the investigation of the contour plots of the main flow properties. Then, we move to a deeper investigation of the flow behavior based on the analysis of temperature and elemental molar fraction profiles extracted in several crucial parts of the computational domain.

In the first part, we address the issue of the influence of finite-rate chemistry on the results of the simulation. To this end, two models have been selected as representative of Earth's atmosphere chemistry (Park [14] and Dunn–Kang [15]). Several numerical experiments have been conducted to assess how the operating pressure drives the flow behavior when one of the two models is used. As a result, we notice that the influence of the finite-rate chemistry is only limited to low pressures (around 5 kPa). Indeed, as the operating pressure is set to higher values, the results obtained under CNEQ with both models are in very good agreement.

In the second part of this section, we move to a deeper investigation of the air plasma behavior. To this end, we present the evolution of the main flow properties along the radial direction at four locations in the computational domain (Fig. 1b): 1) in the inlet zone ($z = 0.005$ m), 2) at the midcoil position ($z = 0.268$ m), 3) at the outlet of the torch ($z = 0.505$ m), and 4) within the chamber ($z = 0.800$ m).

A. Qualitative Analysis of the Results for 5 kPa

In this section, we discuss the influence of the finite-rate chemistry model on the flow behavior. To this end we present temperature and elements concentration both in the torch and in the chamber by means of contour plots. Two of the four operating pressures specified in the preceding section have been selected to perform this study, the lowest (5 kPa) and the highest (30 kPa). Focusing on these two pressures, we will be able to easily show how the differences observed in the flow solution, due to differences in the reaction rates, are visible only in the low-pressure case and disappear when the operating pressure is increased up to 30 kPa. We therefore leave the definition of the pressure limit above which the influence of the finite-rate model becomes negligible to the study performed in the next section. The results to be presented shortly have been obtained under

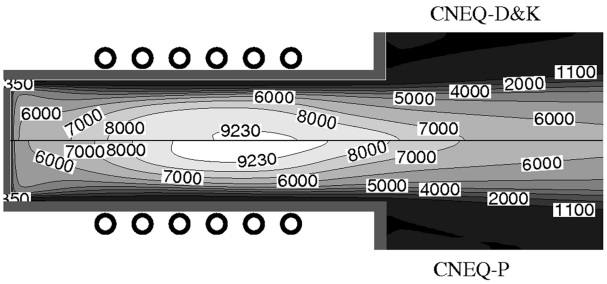

a) Temperature (K) contours obtained with two finite-rate models (5 kPa)

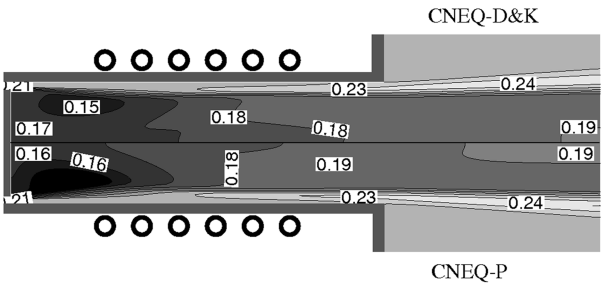

b) Oxygen elemental molar fraction obtained with two finite-rate models (5 kPa)

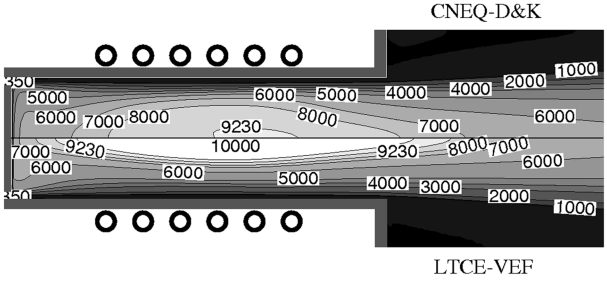

c) Temperature (K) contours, Dunn-Kang model (upper) vs LTCE-VEF (lower) (5 kPa)

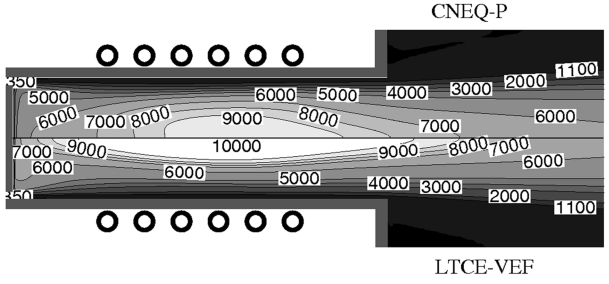

d) Temperature (K) contours, Park model (upper) vs LTCE-VEF (lower) (5 kPa)

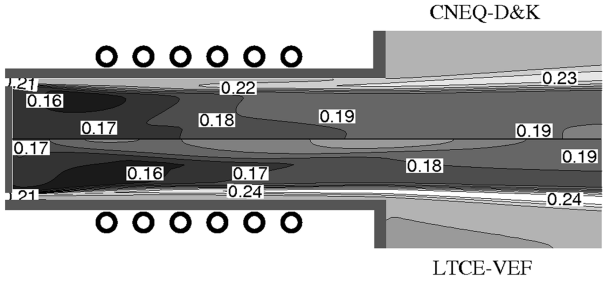

e) Oxygen elemental molar fraction contours, Dunn-Kang model (upper) vs LTCE-VEF (lower) (5 kPa)

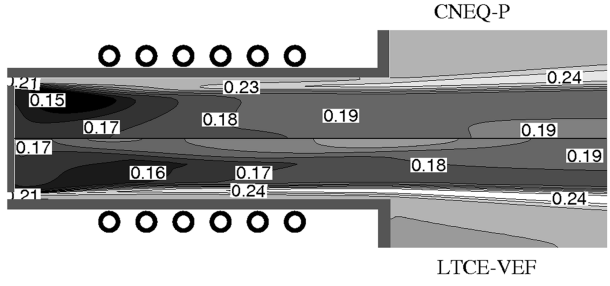

f) Oxygen elemental molar fraction contours, Park model (upper) vs under LTCE-VEF (lower) (5 kPa)

Fig. 2 Air plasma flow within VKI Plasmatron facility under CNEQ, LTCE-CEF, and LTCE-VEF conditions.

LTCE-VEF conditions and under CNEQ using two finite-rate chemistry models: the Park model [14], indicated as CNEQ-P, and the Dunn–Kang model [15] named as CNEQ-D&K.

Each nonequilibrium result is compared with the respective one obtained with the other finite-rate model but also with the result of the simulation carried out under thermochemical equilibrium with variable elemental fraction. This, at the same time, allows for the assessment of the influence of the finite-rate chemistry model and to answer the question of whether or not equilibrium computations give the same results as nonequilibrium simulations for high pressures in the chamber, as already observed in the torch in [8].

In Figs. 2a and 2b we plot the temperature, respectively, the oxygen elemental mass fraction both in the torch and in the chamber. The analysis of these figures reveals the presence of two zones in which the comparison of the results bring us to different conclusions. Indeed, within the torch, we notice that the CNEQ-P and CNEQ-D&K predictions differ considerably, leading to different temperatures and, to a lesser extent, elemental fractions. From Fig. 2 we observe that the Dunn–Kang model predicts a slightly wider hot ($T \geq 6000$ K) region in the torch acting on the structure of the plasma ball. As soon as we move towards the torch exit, we start noticing a rapid dwindling of the disparity between the two predictions which, at least from a qualitative point of view, show the same temperature field in the jet, corresponding to the most interesting part of the flowfield from the point of view of TPM testing.

For what concerns the oxygen elemental fraction, we notice that the finite-rate chemistry model has little influence on the elements concentration field, showing once again that demixing is not a nonequilibrium effect (Fig. 2b).

In Figs. 2c–2f, we present a comparison between the results obtained under chemical nonequilibrium with the Park and Dunn–Kang models with those obtained under chemical equilibrium with variable elemental fractions. In Figs. 2c and 2d we focus on the temperature contours whereas in Figs. 2e and 2f, we investigate the oxygen elemental fraction. As expected, thanks to the analysis performed in [8], the temperature contours obtained under chemical nonequilibrium differ considerably from those obtained with the equilibrium formalism and this for both finite-rate chemistry models. From the oxygen elemental fraction presented in Figs. 2e and 2f we notice a certain difference in the prediction of the elemental concentration field between equilibrium and nonequilibrium even though the order of magnitude of the oxygen variations is the same.

We now move to the analysis of the higher pressure (30 kPa) and we start our analysis presenting, as done for the lower pressure case, the comparison between nonequilibrium results. In Figs. 3a and 3b we present the temperature, respectively, the elemental fraction contours both in the torch and in the chamber. From the analysis of the temperature contours, we notice that at an operating pressure of 30 kPa, the results obtained with the two models are, at least from a qualitative point of view, equivalent. The same conclusion is drawn after inspection of Fig. 3b where attention is focused on the oxygen

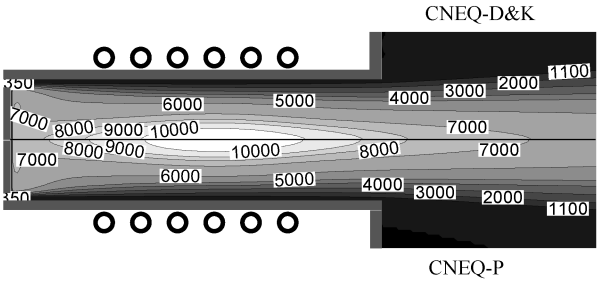

a) Temperature (K) contours obtained with two finite-rate models (30 kPa)

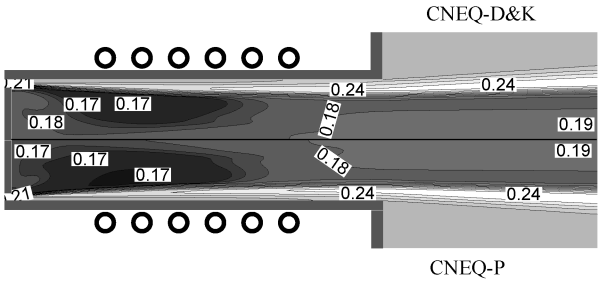

b) Oxygen elemental molar fraction obtained with two finite-rate models (30 kPa)

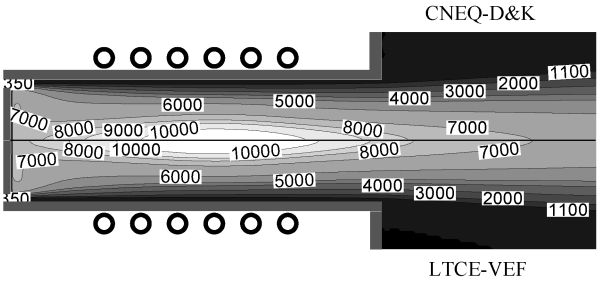

c) Temperature (K) contours, Dunn-Kang (upper) vs under LTCE-VEF (lower) (30 kPa)

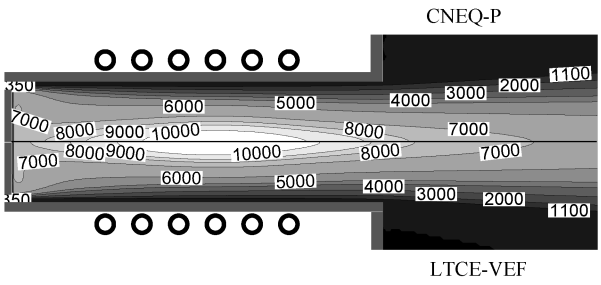

d) Temperature (K) contours, Park (upper) vs LTCE-VEF (lower) (30 kPa)

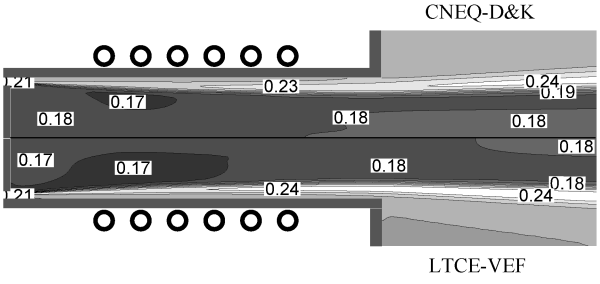

e) Oxygen elemental molar fraction contours, Dunn-Kang (upper) vs LTCE-VEF (lower) (30 kPa)

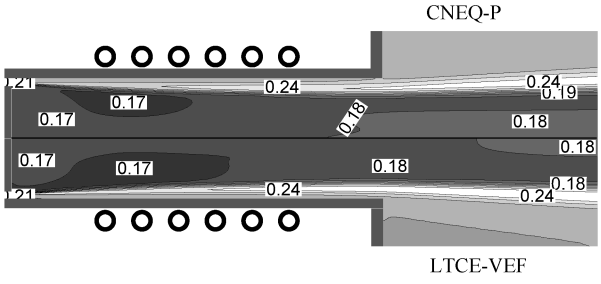

f) Oxygen elemental molar fraction contours, Park (upper) vs LTCE-VEF (lower) (30 kPa)

Fig. 3 Air plasma flow within VKI Plasmatron facility under CNEQ, LTCE-CEF, and LTCE-VEF conditions.

elemental fraction. Differences between the prediction with the Park and the Dunn–Kang models are hardly visible.

In the following, we present the comparison between the previous results with the respective equilibrium computations. The critical analysis of these comparisons will enhance the importance of the previous conclusions. In Figs. 3c–3f we present the direct comparison between the temperature, respectively, the elemental mole fraction contours obtained both under chemical nonequilibrium and equilibrium with variable elemental fraction. From Figs. 3c and 3d we realize that the temperature contours predicted by the simulation of equilibrium conditions coincide with those obtained under chemical nonequilibrium for both finite-rate chemistry models after the last coil. Indeed, some small differences are visible within the torch until the last coil is reached. To further decrease these differences in the torch we just need to increase the operating pressure. On the other hand, at the torch exit, but most importantly in the test chamber, an excellent match is observed. Similar conclusions can be drawn for the elemental composition after inspection of Figs. 3e and 2f.

The results just described have a direct impact on the methodology used for the estimation of the catalytic properties of thermal protection materials. Indeed, thanks to the previous analysis we can argue that for sufficiently high pressures the equilibrium formalism allows for the determination of results, both in the torch and in the chamber, characterized by an accuracy very close to the one we can achieve with nonequilibrium simulations. This conclusion will allow researchers performing inductively coupled plasma flow simulations for the characterization of TPM to obtain accurate results using an equilibrium formulation at a fraction of the cost required to simulate the same conditions under nonequilibrium.

In the next section we firstly provide a validation of the previous analysis, by means of the investigation of the local behavior of the plasma flow, and secondly, we define the pressure limit above which the previous conclusion is applicable.

B. Detailed Analysis

In this section, we present the local evolution of the main flow properties in the four locations specified in the preceding section and for each of the four operating pressures defined in Sec. III. From the qualitative analysis presented in Sec. , we observed that for the low-pressure case some discrepancies are visible between the results obtained under chemical nonequilibrium and equilibrium, whereas for high pressure these differences essentially disappeared. Following this result, we will divide the analysis into two parts: the detailed analysis of the low-pressure case and the parametric study of the pressure influence. In the first part, we present a detailed investigation of the low-pressure case showing the results obtained for several chemical regimes in four locations. This will lead to an accurate description of the spatial evolution of the flow properties and will allow to verify whether, even at a so low operating pressure, a match between equilibrium and nonequilibrium results can be found somewhere in the flow. For what concerns the parametric study of pressure influence, we focus our attention only on the outlet of the chamber. Indeed, as discussed during the previous qualitative analysis, the most interesting part of the flowfield from the point of view of TPM testing is the hot-jet exiting from the torch. Therefore, for this particular location, we will discuss how the operating pressure drives the flow behavior depending on the chemical regime under investigation.

Before starting with the analysis we will spend few words trying to enlighten the main physical effects of the demixing on the temperature and oxygen elemental fraction. As we shall see in the next session (Figs. 4–7) we notice a small influence of this phenomena on the temperature; this can be seen comparing the radial plots in case of LTCE-CEF with the ones carried out in LTCE-VEF, especially in the inlet area next to the symmetry axis. The influence of demixing on the oxygen elemental fraction is, on the contrary, quite important as already pointed out by the previous qualitative analysis. Generally speaking we notice the tendency of the elemental oxygen to diffuse from the area next to the symmetry axis towards the wall.

1. *Low-Pressure Case*

We start presenting the axial evolution of the elemental oxygen mole fraction at 5 kPa in Fig. 4.

Firstly, we focus our attention on the chemical nonequilibrium results in the inlet zone where we notice the presence of a strong

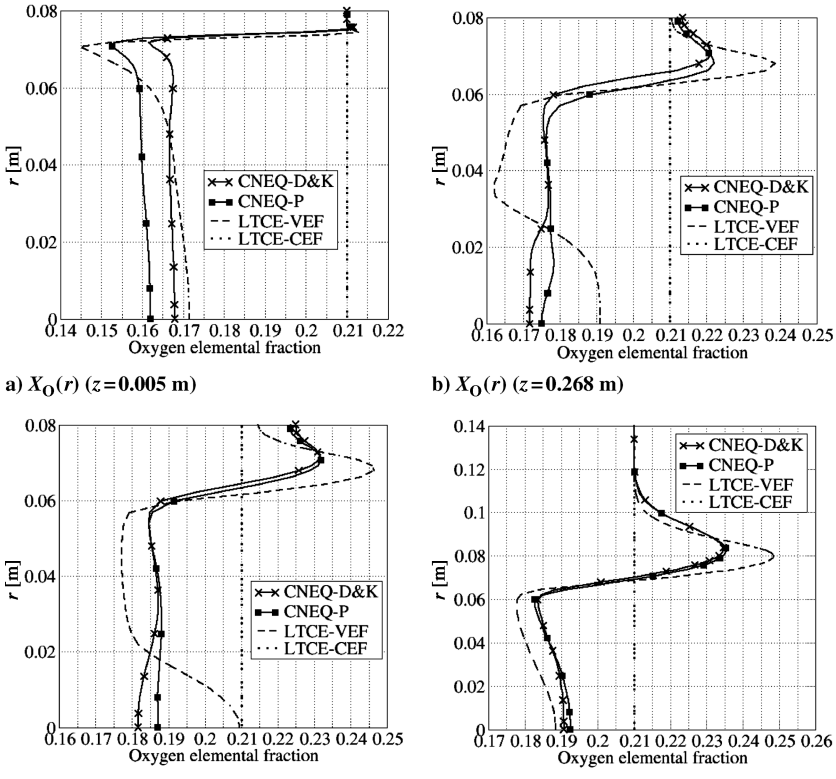

a) $X_O(r)$ ($z = 0.005$ m) b) $X_O(r)$ ($z = 0.268$ m)

c) $X_O(r)$ ($z = 0.505$ m) d) $X_O(r)$ ($z = 0.800$ m)

Fig. 4 Oxygen elemental molar fraction radial profiles at four locations (5 kPa).

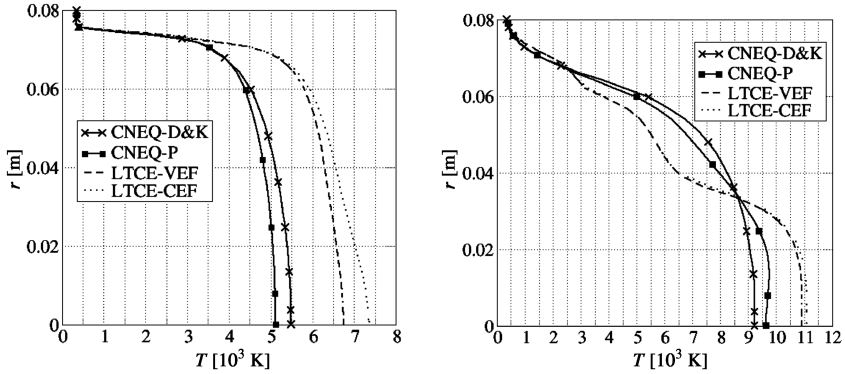

a) $T(r)$ ($z = 0.005$ m) b) $T(r)$ ($z = 0.268$ m)

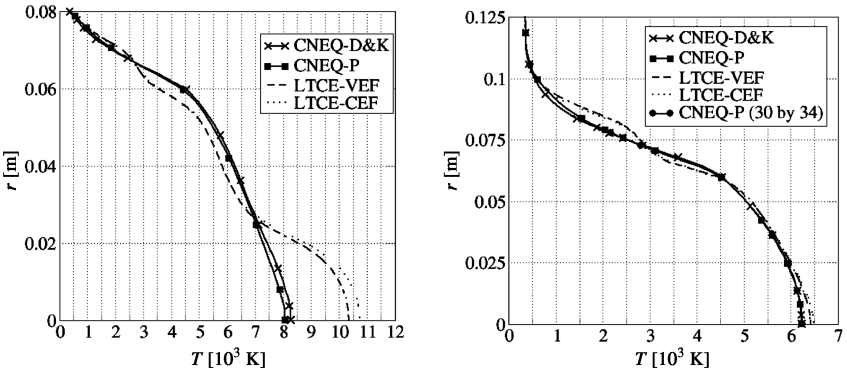

c) $T(r)$ ($z = 0.505$ m) d) $T(r)$ ($z = 0.800$ m)

Fig. 5 Temperature radial profiles at four locations (5 kPa).

depletion of oxygen. In addition, we are now able to show that the chemical nonequilibrium predicts a similar oxygen profile for both finite-rate models. Indeed, from the wall towards the axis we notice a rapid decrease of oxygen concentration followed by a plateau starting around $r \sim 6$ cm. The values of the plateau differ slightly for the two solutions obtained with the Park (∼0.16) and the D&K (∼0.17) models. As we move forward from the inlet (Fig. 4a) to the midcoil position (Fig. 4b), we retrieve similar results as for the

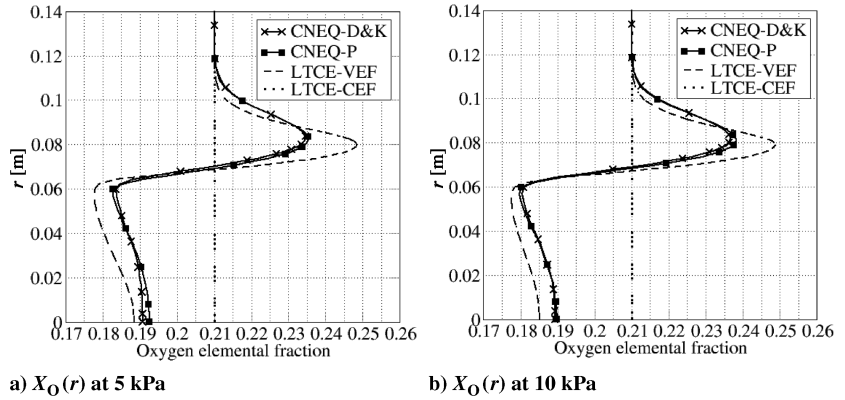

a) $X_O(r)$ at 5 kPa b) $X_O(r)$ at 10 kPa

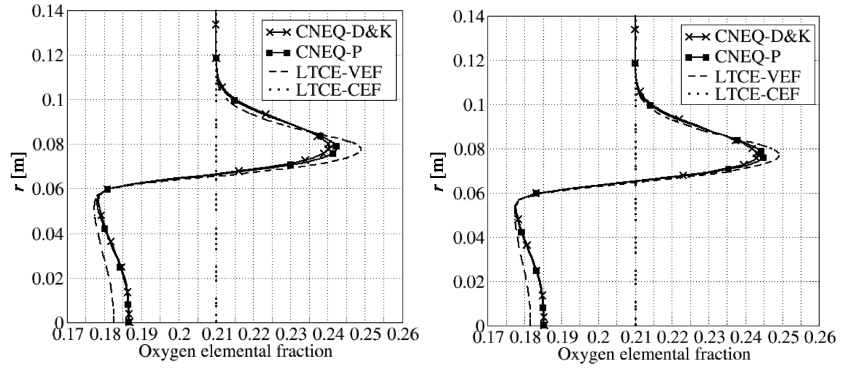

c) $X_O(r)$ at 20 kPa d) $X_O(r)$ at 30 kPa

Fig. 6 Oxygen elemental molar fraction for several operating pressures at $z = 0.8$ m.

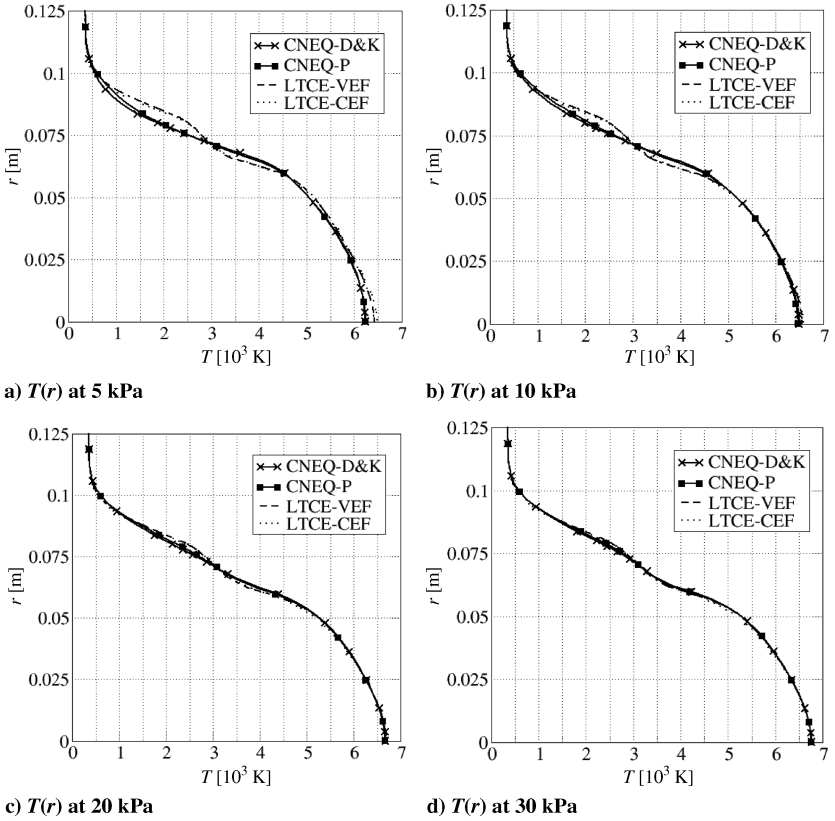

a) $T(r)$ at 5 kPa b) $T(r)$ at 10 kPa

c) $T(r)$ at 20 kPa d) $T(r)$ at 30 kPa

Fig. 7 Temperature profiles for several operating pressures ($z = 0.8$ m).

equilibrium regime and we notice that the discrepancies between the predictions obtained with the two chemical kinetics models decrease with respect to the previous location and remain confined in a region close to the axis. These differences are further decreased when we move to the torch exit (Fig. 4d), where we notice a very good match between the CNEQ-P and the CNEQ-D&K predictions for $r > 0.3$ cm. The small differences observed in the third section vanish (Fig. 4d) during the time needed by the flow to reach the exit of the computational domain. Indeed, from the analysis of Fig. 4d we notice that the elemental fraction profiles obtained with the two models follow the same radial evolution.

Another interesting conclusion about the predictions obtained for different chemical regimes is drawn from the comparison between equilibrium and nonequilibrium results. Indeed, we clearly notice that as we move from the inlet towards the chamber, the nonequilibrium results follow closer and closer the equilibrium ones. Within the torch, we remark that the prediction obtained using the nonequilibrium formalism is characterized by a plateau for $r < 6$ cm and, as we move toward the quartz tube, a peak is observed close to the wall for $r \sim 7$ cm. After the torch, the plateau is stretched, leading to a profile with a minimum for $r \sim 6$ cm, from which the oxygen concentration increases towards the axis, presenting a local extremum with a corresponding value slightly higher than 0.18. In particular, we notice that the predictions of the elemental molar fraction near the axis within the test chamber, obtained with the two formalisms (CNEQ and LTCE-VEF), essentially coincide. This result is of direct application to the determination of catalytic properties of TPS materials because it shows that, even for a low operating pressure, the results obtained with an equilibrium formalism lead to the same elemental fraction around the axis as the one obtained under equilibrium conditions with the two different chemistry models. This local elemental fraction is different from the value corresponding to the inlet and will therefore influence the rebuilding procedure, at least from a conceptual point of view. The importance of this influence will, in general, depend on the operating conditions and especially from the mixture selected as representative of the plasma to be tested.

In Fig. 5, we present the radial temperature profiles in the four locations previously investigated. We start our analysis of the temperature evolution by considering the nonequilibrium results. As for the oxygen elemental fraction we observe that the results obtained with the two models lead to the same temperature profiles beyond the midcoil position. On the other hand, some differences are visible close to the inlet (Fig. 5a) and in the middle of the torch (Fig. 5b). As soon as we move to the exit of the domain (Fig. 5d), the remaining differences gradually disappear. From the comparison between the equilibrium and nonequilibrium results, we immediately draw conclusions similar to those obtained for the elemental fraction. Indeed, within the torch we observe a nonnegligible difference between the equilibrium and nonequilibrium results, especially close to the axis where the equilibrium predictions lead to a higher temperature than what is observed under nonequilibrium. As shown in [8], we notice that the temperature prediction obtained under equilibrium is not strongly influenced by the elemental fraction variations both within and outside the torch. Finally, we clearly observe that, in the chamber (Fig. 5d), the predictions obtained in the four computations are very close, especially for $r > 2$ cm, even if small discrepancies are visible on the axis. The previous results, and in particular the analysis of Figs. 4d and 5d, show that even at low pressure the prediction of the flow behavior in the chamber obtained under nonequilibrium with two finite-rate models, and under equilibrium with variable elemental fraction, are very close.

2. *Parametric Study of Pressure Influence*

We now move to the parametric study of the pressure influence on the flow behavior in the test chamber. The main objective of this analysis is to characterize the flow in the jet at a certain distance downstream of the torch exit. For this purpose we focus on the exit of the computational domain placed 30 cm after the beginning of the chamber. This distance, even if arbitrary, lies in the range of possible locations where the heat flux probe can be placed within the test chamber.

Our analysis is based on the discussion of the results presented in Figs. 6 and 7, where we show the oxygen elemental mole fraction, respectively, the temperature profiles, at the outlet of the domain ($z = 0.8$ m). Observing the profiles presented in Fig. 6, we notice that the results obtained under chemical nonequilibrium with the two finite-rate models are always coincident for each operating pressure. This leads us to the following observation: the use of Park and Dunn–Kang models leads to the same prediction of the radial evolution of the elemental concentration for $z = 0.8$ m. If we consider the comparison between the equilibrium and nonequilibrium results, we remark that the nonequilibrium prediction approaches the equilibrium one as pressure rises. Indeed, for the first two pressures (Figs. 6a and 6b), we notice some differences between the predicted values of the oxygen peak, observed for $r \sim 8$ cm, and in the minimum, located around $r \sim 6$ cm. On the other hand, the values predicted on the axis by the CNEQ and the LTCE-VEF computations are always similar. As pressure is increased (Figs. 6c and 6d), the axial values of the oxygen molar fraction slightly decreases, but most importantly, the remaining part of the oxygen profiles obtained under nonequilibrium starts to follow the equilibrium one (Fig. 6c) and, for the highest pressure, the two predictions almost coincide (Fig. 6d). As a consequence, we can conclude that starting from 10 kPa, numerical simulations carried out under chemical equilibrium lead to results which are easier to perform and nearly as accurate as those obtained under chemical nonequilibrium in the jet for $z \sim 0.8$ m. Indeed, the maximum relative error obtained at 10 kPa (Fig. 6a) is of the order of $\sim$5%. As pressure increases, this error decreases and reaches $\sim$3% at 30 kPa.

The particular radial evolution of the oxygen profiles follows from the oxygen diffusion within the torch described in detail in [8] and briefly recalled hereafter.

Because of the strong temperature gradients in the radial direction, concentration variations and diffusion also mainly act perpendicularly to the wall. Because the atomic oxygen contained inside the plasma ball diffuses faster than the (heavier) molecular oxygen in the low temperature zones adjacent to the wall, we observe a strong increase in the overall fraction of oxygen elements near the wall.

After the torch exit, the form of the profile inside the jet does not change considerably in the axial direction, whereas, along r, after the peak ($r \sim 8$ cm) the oxygen concentration tends toward the constant characteristic value of the relatively cold flow present in the chamber at higher radius ($r > 12$ cm). Each of the graphs presented in Fig. 6 reflects the qualitative analysis presented previously showing that the defect of oxygen observed in the jet is compensated by an excess of oxygen concentrated in the volume between two cylinders. In the highest pressure case (Fig. 6d), this volume is confined between an inner radius $\sim$7 cm and an outer radius $\sim$9 cm.

As for the elemental concentration, the most important part of the temperature profiles corresponds to the zone close to the axis, which is of direct interest for the estimation of the catalytic activity of TPS materials. For this reason, to improve the readability of the graphs to be presented shortly, we present the temperature profiles for $r < 12.5$ cm, knowing that the temperature is almost constant for larger radii. We start our analysis comparing the results obtained under nonequilibrium with two finite-rate models. For all the operating pressures, the use of the Park and Dunn–Kang models for the description of the air finite-rate chemistry brings to the same radial temperature evolution. The differences between equilibrium and nonequilibrium predictions visible in the lowest pressure case (Fig. 7a) gradually disappears as pressure rises. Indeed, for 10 kPa (Fig. 7b) and to 20 kPa (Fig. 7c) some small differences are visible, but they disappear for the highest operating pressure (Fig. 7d). These observations lead us to conclusions similar to those drawn from the analysis of the oxygen elemental fraction. Indeed, starting from 10 kPa the three formalisms CNEQ, LTCE-VEF, and LTCE-CEF predict the same temperature profile. With respect to the oxygen elemental fraction, we anyway notice that the elemental diffusion does not affect the temperature at sufficiently high pressure (>10 kPa).

The results obtained in the framework of the present research activity and therefore the conclusion of this study, depend on the geometrical characteristics and the operating conditions of the ICP facility investigated. In particular, the power injected into the plasma, the frequency of the current running into the coils, and the mass flow together with the torch size might influence the pressure threshold above which the flow reaches equilibrium conditions [16,17]. To assess the influence of these parameters in a qualitative way a deep analysis should be carried out which could be based on the identification of some dimensional parameters governing the flow behavior in the purpose of eventually defining some scaling laws as for example suggested in [30].

IV. Conclusions

In this paper, we presented the analysis of air plasma flows both in the torch and in the chamber of the VKI Plasmatron for four operating pressures ranging from 5 to 30 kPa. The results obtained for this geometrical configuration have been produced using three formulations: chemical nonequilibrium and equilibrium with both constant and variable elemental fractions. In addition, two finite-rate models have been used to obtain the nonequilibrium results. The analysis of these results leads us to the following conclusions:

1) For the low-pressure case (5 kPa), we observe a certain influence of the finite-rate chemistry model on the prediction of the flow behavior within the torch. This influence was found to decrease considerably after the torch, leading to almost negligible differences at the end of the computational domain placed $\sim$30 cm after the torch.

2) From the comparison of the equilibrium and the nonequilibrium results, we notice that the flow in the torch is indeed in nonequilibrium for the low-pressure case (5 kPa). The degree of nonequilibrium depends on the position, decreases as we move toward the exit of the torch, and is sensibly reduced in the jet. There, the nonequilibrium results are rather close to the equilibrium ones, provided that elemental demixing is taken into account.

3) As pressure rises, the differences between the predictions obtained with the two finite-rate models sharply decrease in the whole flowfield. They are very small for the low-pressure case (5 kPa) and they become negligible afterwards.

4) By increasing the operating pressure, we act directly on the relation between nonequilibrium and equilibrium results. Indeed, the predictions obtained in the jet using both finite-rate chemistry models approach the equilibrium results already in the lowest pressure case. Then, if pressure is further increased, the differences between the equilibrium and nonequilibrium predictions decrease and become negligible at 10 kPa.

In light of the preceding observations, we can therefore conclude that, for the purpose of thermal protection materials testing, for sufficiently high pressures, the prediction of the flow physico-chemical state in the jet obtained under equilibrium conditions where elemental demixing is taken into account is as accurate as the one obtained under nonequilibrium conditions. In the present study, the pressure limit above which the previous conclusion is valid has been observed to be 10 kPa.

References

[1] M. Capitelli, G. C., and Armenise, I., "State to State Electron and Vibrational Kinetics in One Dimensional Nozzle and Boundary Layer Flows," *Physico-Chemical Models for High Enthalpy and Plasma Flows*, Vol. 1, von Kármán Institute, Rhode-Saint-Genèse, Belgium, July 2002, p. 21.

[2] Pierrot L. C., Laux, C. O., and Kruger, C. H., "Vibrationally-Specific Collisional-Radiative Model for Non-Equilibrium Nitrogen Plasmas," AIAA Paper 1998-2664, 1998.

[3] Laux, C., "Radiation and Nonequilibrium Collisional Radiative Models," *Physico-Chemical Models for High Enthalpy and Plasma Flows*, Vol. 1, Rhode-Saint-Genèse, Belgium, July 2002, p. 55.

[4] Vasil'evskii, S. A, Kolesnikov, A. F., and Yakushin, M. I., "Mathematical Models for Plasma and Gas Flows in Induction Plasmatrons," *Molecular Physics and Hypersonic Flows*, edited by M. Capitelli, Kluwer, Dordrecht, The Netherlands, 1996, pp. 495–504.

[5] Murphy, A. B., "Demixing Due to Frictional Forces in an Electric Arc," *Physical Review Letters*, Vol. 73, 1994, pp. 1797.

[6] Rini, P., "Analysis of Differential Diffusion Phenomena in High Enthalpy Flows," Ph.D. Thesis, von Kármán Institute for Fluid Dynamics, Rhode-St-Genèse, Belgium, March 2006.
[7] Park, C., *Nonequilibrium Hypersonic Aerothermodynamics*, John Wiley and Sons, New York, 1989.
[8] Rini, P., Vanden Abeele, D., and Degrez, G., "Elemental Demixing in Inductively Coupled Air Plasmas at High Pressures," *Journal of Thermophysics and Heat Transfer*, Vol. 20, No. 1, 2006, pp. 31–40.
[9] Bottin, B., Chazot, O., Carbonaro, M., Van Der Haegen, V., and Paris, S., "The VKI Plasmatron Characteristics and Performace," NATO RTO-EN 8, St.-Genesius-Rhode, Belgium, Oct. 1999.
[10] Kolesnikov, A. F., "Extrapolation from High Enthalpy Tests to Flight Based on the Concept of Local Heat Transfer Simulation," NATO RTO-EN 8, St.-Genesius-Rode, Belgium, Oct. 1999.
[11] Bukowski, J. D., Graves, D. B., and Vitello, P., "Two-Dimensional Model of an Inductively Coupled Plasma with Comparison to Experimental Spatial Profiles," *Journal of Applied Physics*, Vol. 80, No. 5, 1996, pp. 2614–2623.
[12] Sarma, G. S. R., "Physico-Chemical Modeling in Hypersonic Flow Simulation," *Progress in Aerospace Sciences*, Vol. 36, No. 3, April 2000, pp. 281–349.
[13] Vincenti, W., and Kruger, C., *Introduction to Physical Gas Dynamics*, John Wiley and Sons, New York, 1965.
[14] Park, C., "Review of Chemical-Kinetic Problems of Future NASA Mission, 1: Earth Entries," *Journal of Thermophysics and Heat Transfer*, Vol. 7, July–Sept. 1993, pp. 385–398.
[15] Gnoffo, P. A., Gupta, R. N., and Shinn, J. L., "Conservation Equations and Physical Models for Hypersonic Air Flows in Thermal and Chemical Non-Equilibrium," NASA Technical Paper 2867, 1989.
[16] Panesi, M., Rini, P., and Chazot, O., "Numerical Simulation of Non-Equilibrium Plasma Flows," VKI-DC 2005-23, von Kármán Institute for Fluid Dynamics, St.-Genesius-Rode, Belgium, 2005.
[17] Vanden Abeele, D., "Contribution à la modélisation numérique de torches à plasma d'induction," Ph.D. Thesis, von Kármán Institute for Fluid Dynamics, Rhode-St-Genèse, Belgium, Oct. 1998.
[18] Magin, T., "A Model for Inductive Plasma Wind Tunnels," Ph.D. Thesis, von Kármán Institute for Fluid Dynamics, Rhode-St-Genèse, Belgium, June 2004.
[19] Magin, T., Vanden Abeele, D., and Degrez, G., "An Implicit Multiblock Solver for Inductive Plasma Flows," AIAA Technical Paper 2000-2480, June 2000.
[20] Thoemel, J., Magin, T., and Chazot, O., "Numerical Parametric Study of a Plasma Jet Re-Entry Application." VKI-SR 2004-46, von Kármán Institute for Fluid Dynamics, St.-Genesius-Rode, Belgium, 2004.
[21] Hirschfelder, J. O., Curtiss, C. F., and Bird, R. B., *Molecular Theory of Gases and Liquids*, Wiley, New York, 1964.
[22] Bottin, B., Vanden Abeele, D., Carbonaro, M., Degrez, G., and Sarma, G. S. R., "Thermodynamic and Transport Properties for Inductive Plasma Modeling," *Journal of Thermophysics and Heat Transfer*, Vol. 13, No. 3, 1999, pp. 343–350.
[23] Gupta, R. N., Yos, J. M., Thompson, R. A., and Lee, K. P., "A Review of Reaction Rates and Thermodynamic and Transport Properties for an 11-Species Air Model for Chemical and Thermal Non-Equilibrium Calculations to 30 000 K," NASA Reference Publication 1232, Aug. 1990.
[24] Sutton, K., and Gnoffo, P. A., "Multi-Component Diffusion with Application to Computational Aerothermodynamics," AIAA Technical Paper 98-2575, June 1998.
[25] Barbante, P. F., Degrez, G., and Sarma, G. S. R., "Computation of Nonequilibrium High-Temperature Axisymmetric Boundary-Layer Flows," *Journal of Thermophysics and Heat Transfer*, Vol. 16, No. 4, 2002, pp. 490–497.
[26] Barbante, P. F., "Accurate and Efficient Modeling of High Temperature Nonequilibrium Air Flows," Ph.D. Thesis, von Kármán Institute for Fluid Dynamics, Rhode-Saint-Genèse, Belgium, 2001.
[27] Yos, J. M., "Approximate Equations for the Viscosity and Translational Thermal Conductivity of Gas Mixtures," Avco Corporation, Contract Report AVSSD-0112-67-RM, Wilmington, MA, April 1967.
[28] Vanden Abeele, D., and Degrez, G., "Efficient Computational Model for Inductive Plasma Flows," *AIAA Journal*, Vol. 38, No. 2, 2000, pp. 234–242.
[29] Mitchner, M., and Kruger, C., *Partially Ionized Gases*, John Wiley and Sons, New York, 1973.
[30] Vanden Abeele, D., and Degrez, G., "Similarity Analysis for the High-Pressure Inductively Coupled Plasma Source," *Plasma Sources Science and Technology* , Vol. 13, No. 1, 2004, pp. 680–690.